applied sciences

MDPI

Article

Study on the Influencing Factors of the Atomization Rate in a Piezoceramic Vibrating Mesh Atomizer

Qiufeng Yan [1,*], Wanting Sun [2] and Jianhui Zhang [3]

1 School of Electrical Engineering, Nantong University, Nantong 226019, China
2 School of Materials Science and Engineering, Harbin Institute of Technology, Harbin 150001, China; sunwt_hit@126.com
3 College of Mechanical and Electrical Engineering, Guangzhou University, Guangzhou 510006, China; zhangjh@nuaa.edu.cn
* Correspondence: yanqf@nuaa.edu.cn; Tel.: +86-1811-222-3232

Received: 29 February 2020; Accepted: 1 April 2020; Published: 2 April 2020

Abstract: On the basis of previous study in our research group, the phenomenon of the dynamic tapered angle was founded, the occurrence of atomization is regarded to derive from the combined effects of the dynamic variation of the micro-tapered aperture, and the difference between forward and reverse flow resistance has been explained by both theories and experiments. It has been revealed that the main influencing factors of the atomization rate are driving voltage, driving frequency, and so on, while the root causes of the various atomization rates still need to be further clarified. In this paper, a micro-tapered aperture worked as a micron-sized tapered flow tube valveless piezoelectric pump in periodic variation. The working principle of such a micro-tapered aperture atomizer was analyzed in detail, and the corresponding formula of the atomization rate was also established. Through measuring the atomization rates at different working frequencies (f), it was established that when the f was set as 122 kHz, the atomization rate reached a maximum value. By building the relationship between the atomization rate and voltage at a fixed resonance frequency, it can be seen that the atomization rate increased with the increase of driving voltage. Subsequently, in order to measure their atomization rates, the micro-tapered apertures of three different outlet diameters were applied, so that the atomization rate was enhanced with the increase of the micro-tapered aperture diameter. Moreover, through examining the atomization rates at different temperatures, it was observed that the atomization rate rose with increasing temperature; while changing the liquid concentration, the atomization rate was also enhanced by the increase in its concentration. Apparently, the impact factors including working frequency, driving voltage, outlet diameter, temperature, and liquid concentration all exert some effects on the atomization rate. It is worth noting that at the first stage, these influence factors indirectly work on the micro-tapered aperture structure or flow state, followed by further effects on the flow resistance. As above-mentioned, in this work, we considered that the root cause influencing the atomization rate in a piezoceramic vibrating mesh atomizer can be attributed to the flow resistance.

Keywords: micro-tapered aperture; pumping effect; flow resistance; atomization rate

1. Introduction

Piezoelectric injection and atomization devices are widely applied in inhalation therapy [1], dust collection [2], preparation of microcapsule [3], printed circuits [4], precise surface coating [5], 3D prototyping [6], spray drying [7], spray cooling [8], inkjet printing [9], and many other fields. Specifically, the micron-sized droplet technique, with the characteristics of stable injection and full dispersion, constitutes an important development direction in these fields [10]. To realize the above-mentioned objectives, surface acoustic wave atomizer [11] and static mesh atomizer [12] can suffer high pressure across the whole system, which inevitably results in high-energy consumption, high cost, and high loss. Furthermore, structures of this type have a low energy utilization rate in which their atomization process is random and uncontrollable, and are also extremely inconvenient to carry and practical use [13].

In light of this, Maehara et al. [14] invented an atomizing film that uses a high-frequency piezoelectric ceramic ring to drive the disperser with a micro-tapered aperture. This type of atomizer can effectively solve problems such as low energy utilization rate, large droplet size, and high dispersion degree [15]. Consequently, research on these types of atomizer have attracted tremendous attention from many scholars. In 1997, Perçin et al. [16] proposed a piezoelectric atomizer where the shaft excited on a circular film by a flexural transducer was stacked into a resonant film to generate atomization. Subsequently, the formation of droplets, which verified the atomization performance of the atomizer, was simulated when the intermediate medium was selected as water, ink, powder, and photoresist, respectively [17]. A control model of the atomizer during photolithography was established by Roche et al. [18], and a similar atomizer was developed by Lam et al. [19] and they took advantage of it for PMN-PT single-crystal spraying. In 2008, Shen et al. [20] studied an atomizer with a cymbal-type high-power driver, where the atomizing device was mainly comprised of a ring-shaped piezoelectric vibrator and a cymbal-shaped nozzle plate. The atomizer could generate droplets with these parameters of a mass median aerodynamic diameter of 4.07 μm, operating frequency of 127.89 kHz, and an atomization rate of 0.5 mL/min [21]. The condition of a stable atomization rate plays a vital role in the application and promotion of the piezoceramic vibrating mesh atomizer, and thus is particularly important for studies on the influencing factors of the atomization rate in a micro-tapered aperture atomizer. Atomizers of this type were subjected to spray cooling by Chen [22], and it was found that the efficiency of spray cooling was closely related to the atomization rate, and that atomization rate is in turn related to aperture diameter. The micro-tapered aperture micro-atomizing film was used by Taso [23] to invent a simple piezoelectric ring micro-fluidic splitter, and was also introduced in both the mass spectrometry (MS) and deposited the sample on the target substrate by means of a spray. The micro-tapered aperture atomizer was performed on the atomizer in spray cooling by Cai et al., and the results showed that the atomization rate had a linear relationship with the cooling performance [24,25]. The atomization rate plays a significant role in the piezoceramic vibrating mesh atomizer. In particular, it is used in some important application fields, for instance, spray cooling [26], inkjet printing [27], inhalation therapy [28], and many other aspects. Up until now, the influence of driving frequency and voltage on atomization rate has only been considered in some references [29,30], but the impact factors are usually ignored. Herein, it is quite necessary to investigate the influencing factors of the atomization rate in the piezoceramic vibrating mesh atomizer, and explore the key working mechanisms.

After investigating the piezoceramic vibrating mesh atomizer, our research group discovered the phenomenon of the dynamic tapered angle [31]. Meanwhile, its presence via a series of experiments was conducted and the pumping effect of a dynamic tapered angle was revealed, which explains why a piezoceramic vibrating mesh atomizer can realize atomization.

This study aimed to analyze in depth the root cause influencing the atomization rate. First, a micro-tapered aperture in periodic variation can be considered as a micron-sized tapered flow tube valveless piezoelectric pump. Second, according to this, this work concentrated on the principle of atomization, and the formula of the atomization rate was deduced. Additionally, the influencing factors of the atomization rate in a piezoceramic vibrating mesh atomizer will be reduced, and the influence of the driving voltage, driving frequency, aperture outlet diameter, liquid temperature, and liquid concentration on the atomization rate will be discussed systematically. Finally, it is expected that the root causes influencing the atomization rate responsible for the variation of the flow resistance will be explored.

2. Structure and Theoretical Analysis of the Piezoceramic Vibrating Mesh Atomizer

The micro-tapered apertures of the piezoceramic vibrating mesh atomizer is machined in the middle of the disperser. In addition, the piezoelectrics are required to be machined into a circular ring. In this section, the structure of the piezoceramic vibrating mesh atomizer is given, and the atomization mechanism of this type atomizer is analyzed.

2.1. Structure

Figure 1 shows a schematic of the piezoceramic vibrating mesh atomizer. The atomizer is composed of a liquid container, atomizing sheet, and liquid storage chamber, in which the atomizing sheet is bonded by the use of AB adhesive. The liquid container is made by 3D printing technology. The piezoelectric ring is bonded tightly to the disperser, and then the inverse piezoelectric effect of the PZT is used to drive the disperser, leading to atomization and ejection. During this operation, the small side of the micro-tapered apertures is exposed to the air, while the large side of the micro-tapered apertures is immersed in the liquid. Under the drive of AC voltage, the atomizing plate will generate a kind of periodic reciprocating motion, which will act on the liquid to form the phenomenon of atomization.

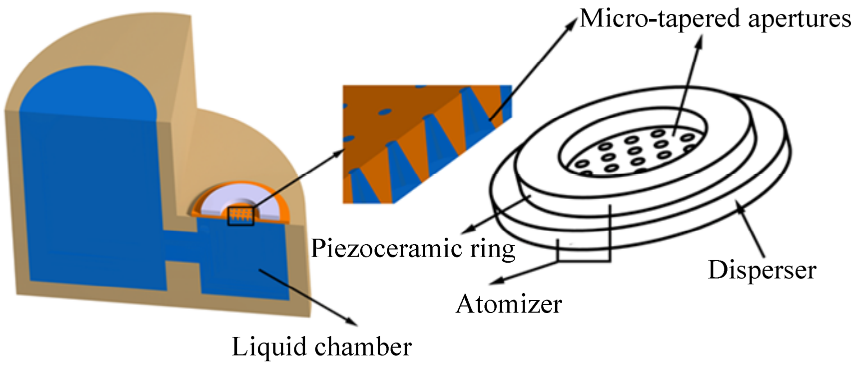

Figure 1. Illustration of the atomizer structure with a piezoceramic vibrating mesh atomizer [31].

2.2. Theoretical Analysis

As indicated by the results in a previous study, when driven by an AC signal, the micro-tapered aperture experiences constant variations in its volume and tapered angle as well as its forward and reverse flow resistance. Such periodic fluctuation of the micro-tapered aperture's volume, combined with the difference between the forward and reverse flow resistance, create a pumping effect, which causes the one-way flow of liquid and thus results in atomization. Olsson et al. [32] compared the numerical calculation of tapered flow with the results obtained in [33]. This indicated that the characteristics of flow resistance in micron-sized divergence/convergence were similar to those for normal sizes. For this reason, the atomization process of the liquid was considered as the working process of a valveless piezoelectric pump [34]. In another way, the variation of the micro-tapered aperture volume is considered to be changed with a piezoelectric vibrator volume in the tapered flow tube valveless piezoelectric pump, and the micro-tapered aperture is processed as the tapered flow tube of the tapered flow tube valveless piezoelectric pump. Driven by a periodic signal, the micro-tapered aperture experiences dynamic variations, and subsequently forms a micron-sized tapered flow tube valveless piezoelectric pump.

For the purpose of this study, as shown in Figure 2a, the liquid flow from the inlet to outlet was defined as forward flow, and the liquid flow from the outlet to inlet as reverse flow is also denoted. According to this definition, the forward and reverse flow resistances of the micro-tapered aperture are represented as ξ_+ and ξ_-, respectively. Considering that the tapered angle of the micro-tapered aperture and its forward-reverse flow resistance varies constantly, their relationship must be expressed in the form of mean flow resistance. The forward mean flow resistance and reverse mean flow resistance of the micro-tapered aperture are shown as follows:

$$\overline{\xi(\chi)_+} = \frac{\int\limits_{\chi\to\infty} \xi(\chi)_+ d\chi}{\chi} \tag{1}$$

$$\overline{\xi(\chi)_-} = \frac{\int\limits_{\chi\to\infty} \xi(\chi)_- d\chi}{\chi} \tag{2}$$

where and respectively represent the forward and reverse transient flow resistance of the micro-tapered aperture.

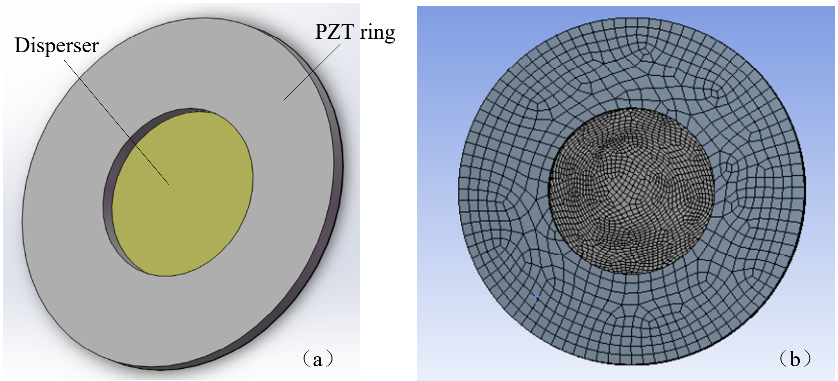

Figure 2. Model and mesh generation of piezoelectric vibrator (**a**) Piezoelectric vibrator model. (**b**) Grid division of piezoelectric vibrator model.

According to the previous study [31], the variation of the micro-tapered aperture volume can be expressed as:

$$\begin{aligned} \Delta V_d &= \iiint\limits_{\Omega} [2z(f_{yy} + f_{xx} + f_y^2 f_{xx} \\ &\quad -2f_x f_y f_{xy} + f_x^2 f_{yy})m^{-1}]dV \end{aligned} \tag{3}$$

Thus, the atomization rate incurred by the pumping effect of the micro-tapered aperture can be expressed as:

$$Q = \Delta V_d f n \frac{\overline{\xi(\chi)_+} - \overline{\xi(\chi)_-}}{2 + \overline{\xi(\chi)_+} + \overline{\xi(\chi)_-}} \tag{4}$$

where ΔV_d represents the variation of the micro-tapered aperture volume in a given period; f represents the driving frequency of the piezoelectric vibrator; and n represents the number of micro-tapered apertures on an atomizing film. As seen from the above formula, the variation of the micro-tapered aperture volume, driving frequency, and the flow resistances of the micro-tapered apertures all exert some influence on the atomization rate.

3. Simulation and Experiments of Vibration Characteristics of Atomizer

In order to obtain the resonant frequency of the piezoceramic vibrating mesh atomizer, the vibration characteristics of the piezoelectric vibrator was simulated by ANSYS software, and the Polytech PSV-300F-B was used to measure the corresponding actual numerical values.

3.1. Simulation

Figure 2 shows the model and mesh generation of the piezoelectric vibrator. As shown in Figure 2a, the gray part is the PZT ring, and the yellow part is the disperser. Table 1 provides the material and geometric parameters of the piezoceramic vibrating mesh atomizer. In this section, the data presented in Table 1 will be adopted for modal analysis of the piezoelectric vibrator.

Table 1. Material and geometric parameters of the piezoceramic vibrating mesh atomizer.

Material	Density (kg/m^3)	Elastic Modulus (Gpa)	Poisson	Inner/Outer Ring Diameter (mm)	Thickness (mm)
PZT	7500	7.65 × 10ˆ10	0.32	7.69/15.96	0.63
Stainless steel	8000	200	0.30	15.96	0.05

Figure 3 shows the simulation diagram of the vibration mode of the piezoelectric vibrator. The simulation results showed that the vibration frequencies of the piezoceramic vibrating mesh atomizer were 22.989 kHz, 83.668 kHz, 122.41 kHz, and 142.07 kHz, respectively. When the piezoelectric vibrator worked at a different resonance frequency, the vibration amplitude became larger, the pump effect was more obvious, thus it was easier to obtain a better atomization effect.

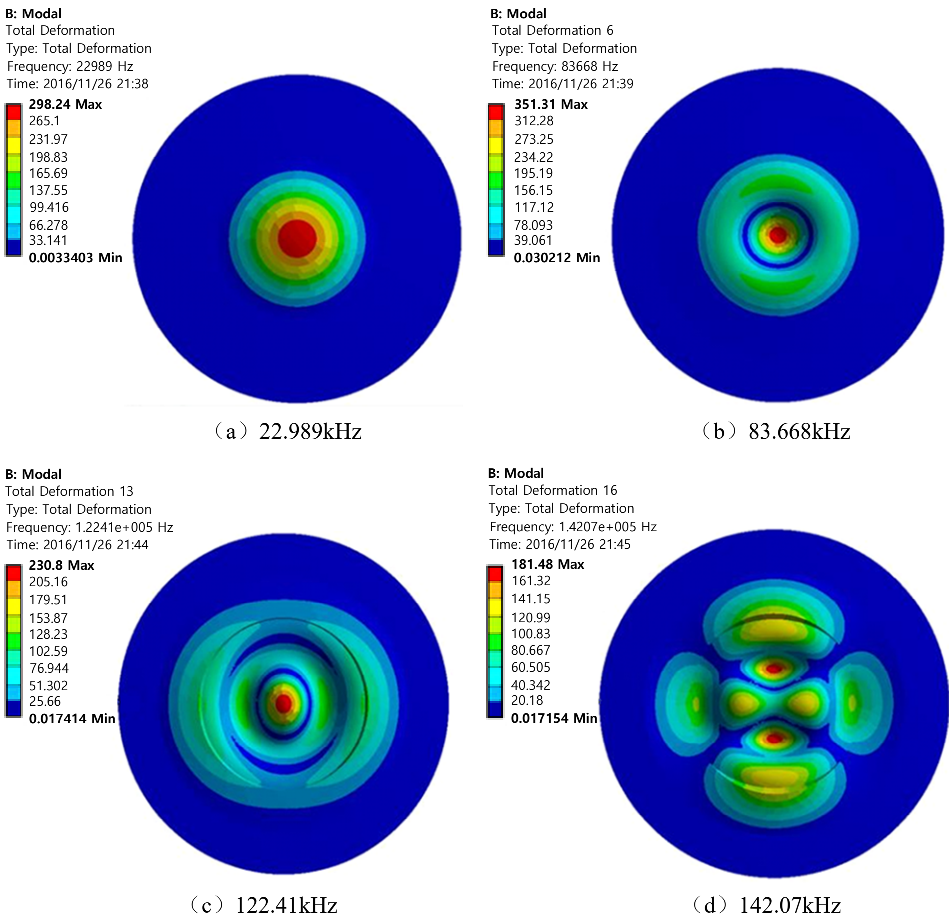

Figure 3. Simulation diagram of the vibration mode of a piezoelectric vibrator.

3.2. Experiment

Figure 4 shows the photograph of the equipment used for measuring the vibration mode of the piezoelectric vibrator. The power amplifier was used to provide the excitation signal during measurement.

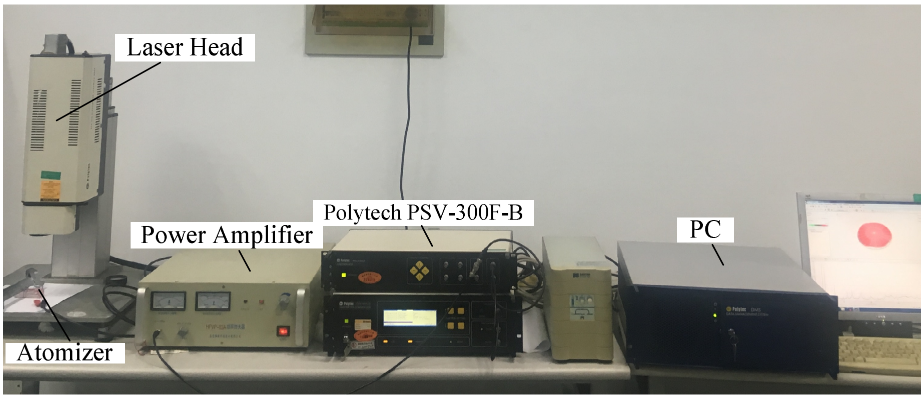

Figure 4. Photograph of the equipment for measuring the vibration mode of the piezoelectric vibrator [29].

Figure 5 shows the frequency sweep curves of the vibration velocity and amplitude magnitude. It can be seen that the change trend of the vibration velocity and amplitude is nearly consistent. The experimental results showed that the resonance frequency of the piezoceramic vibrating mesh atomizer was set as 15.9 kHz, 78.2 kHz, 106.1 kHz, 116.5 kHz, 121.1 kHz, and 148.3 kHz, respectively. Compared to the previous simulation results, it suggests that there were another two resonance points at 106.1 kHz and 116.5 kHz in the experimental results, respectively. There were still some deviations in the corresponding resonance points between the simulation and experimental curves. The reasons for these deviations in the simulation and experimental data can be explained as follows: the finite element simulation is an ideal state, whereas the experimental process is inevitably interfered by some external influencing factors such as errors in measurement.

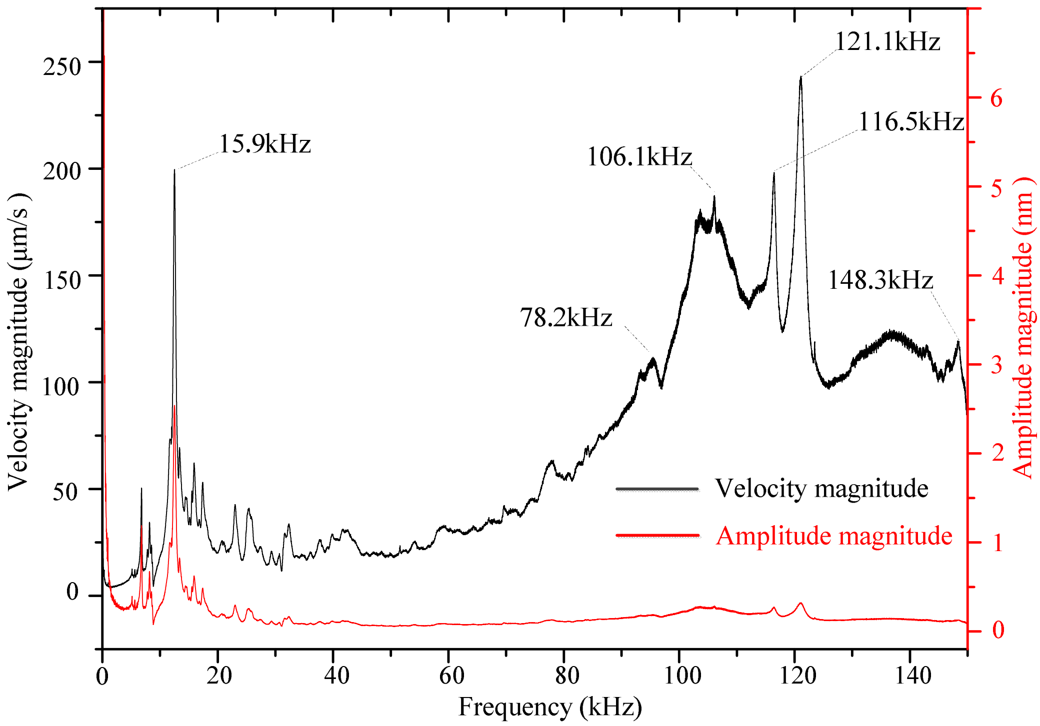

Figure 5. Frequency sweep curves of the vibration velocity and amplitude magnitude [29].

Figure 6 shows the vibration modes of the resonance points. As seen from Figure 6a,b, the resonance frequencies were set as 15.9 kHz and 78.2 kHz, respectively, while the atomization could only be produced under the condition of high frequency vibration. The atomization could not be generated at other lower resonance points. As shown in Figure 6c, the resonance frequency increased to 106.1 kHz. At this resonance point, both the vibration amplitude and vibration speed increased, thus the pump effect gradually forms, and ultimately, micro atomization is produced. Figure 6d shows the evidence that the resonance frequency became higher with a value of 116.5 kHz. As the corresponding vibration amplitude and pump effect are further increased, the atomization rate will also increase. As shown in Figure 6e, at the resonance frequency point of 121.1 kHz, the vibration velocity and frequency of the piezoelectric vibrator reached the maximum. Simultaneously, the volume change of the micro-tapered aperture located in the center of the atomizing plate also reached a maximum, and the pump effect was the strongest with the maximum atomizing rate achieved. However, as the working resonance frequency reached the largest with a value of 148.3 kHz, as shown in Figure 4, it implies that the amplitude of the piezoelectric vibrator is very small at this time, leading to the decrease in the volume change of the micro-tapered aperture, thereby the resulting pump effect is relatively weak with an atomization rate lower than the state at 121.1 kHz.

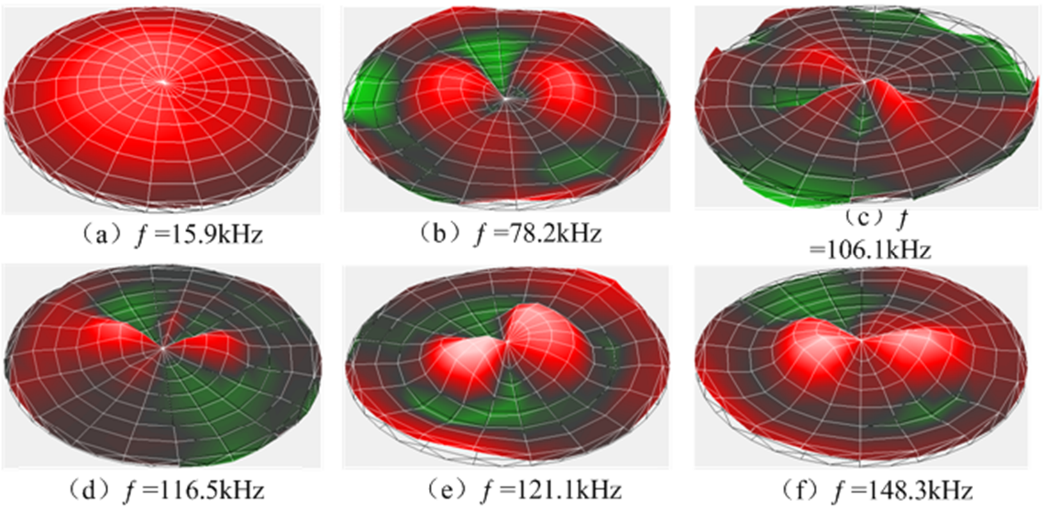

Figure 6. Vibration modes of resonance points [29].

4. Experimental Details of Atomization Rate

In this study, the process of making an ultrasonic atomizer can be described as follows. First, there were about 400 micro-tapered apertures processed on the middle bulge of an atomizing film via laser technology. Second, a circular piezoelectric ceramic was attached to the disperser. Finally, a conductor was welded on the position between the piezoelectric ceramic ring and disperser.

Figure 7a shows the atomizing film structure used in this study, which consisted of a piezoelectric ceramic ring, a disperser with a micro-tapered aperture, and the micro-tapered aperture group on the substrate in the middle tapered blank part. Figure 7b,c show the front view and back view of the atomizing film, respectively. During atomization progress, the surface in Figure 7c comes into contact with the liquid chamber, while the surface, as shown in Figure 7b, makes contact with the external environment. The description for the specific parameters of the atomizing film is provided as follows: piezoelectric ceramic ring with an outer diameter of 15.96 mm; inner diameter of 7.69 mm; thickness of 0.63 mm; disperser with a diameter of 15.96 mm; and thickness of 0.05 mm. The measurements of the outlet diameter and inlet diameter of the micro-tapered aperture were performed on the electron microscope, and the specific parameters are given in the Results and Discussion.

Figure 8 shows the equipment of the atomization rate measurement. During the experimental progress, a signal generator and power amplifier were utilized to supply power to the atomizer, and an oscilloscope was used to control the driving signal. The atomizer was placed on a high-precision analytical balance to measure the liquid's decrease in the liquid chamber of the atomizer after 1 min.

The decrease in the amount of liquid is the atomization volume in an atomizer per minute, that is, the definition of the atomization rate.

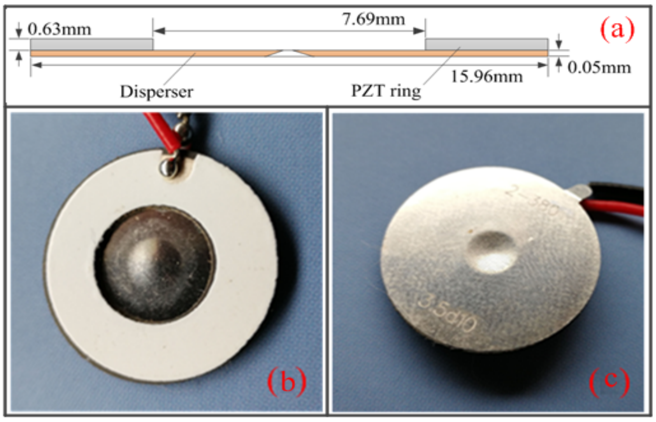

Figure 7. The morphology of the atomizing film. (**a**) Schematic diagram of the atomizing film structure; (**b**) front view of the atomizing film; (**c**) back view of the atomizing film [31].

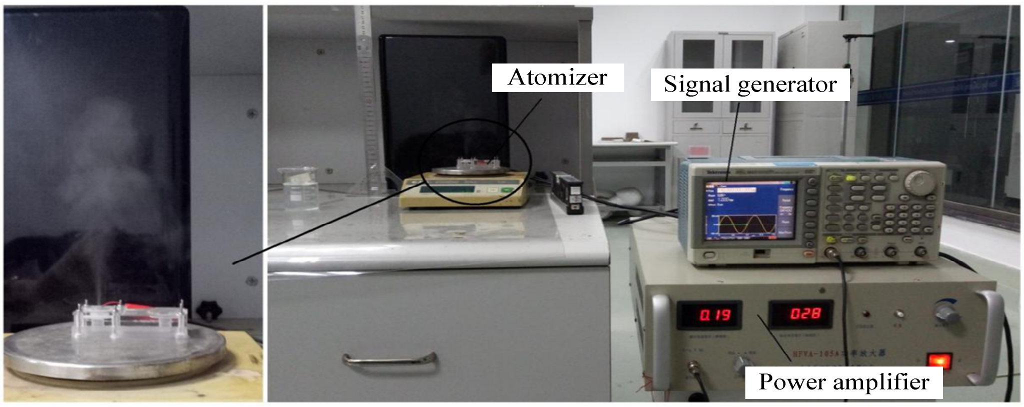

Figure 8. The equipment used for the measurement of the atomization rate.

In this study, the atomization rate represents the weight of the liquid atomized during one minute. During the test of the atomization rate, the atomizer is placed on a high-precision analytical balance, and the stopwatch is used for timing the power supply of the voltage to the atomizer. After one minute, the supplying voltage to the atomizer and the atomization rate stopped being collected. Therefore, the atomization rate was obtained by measuring the reduction of the liquid amount in the liquid chamber per minute using a high-precision analytical balance.

5. Results and Discussion

Figure 9 shows the atomization rate results measured with an interval of 2 kHz within the frequency range of 100–150 kHz at driving voltages of 100 V, 120 V, and 140 V, respectively. The liquid used in the experiment was pure water at room temperature (25 °C), and the pore diameter of the micro-tapered aperture was 12 µm. It can be observed that the atomization rate had a total of four peak points located at f_1 = 106 kHz, f_2 = 116 kHz, f_3 = 122 kHz and f_4 = 148 kHz, respectively. Table 2 shows the atomization rates at different resonance frequencies, when the driving voltage was set at 120 V. The atomization rates at the three driving voltages reached a peak when the driving frequency was f = 122 kHz. The atomization rate was 2.48 mL/min, 3.06 mL/min, and 3.18 mL/min, respectively.

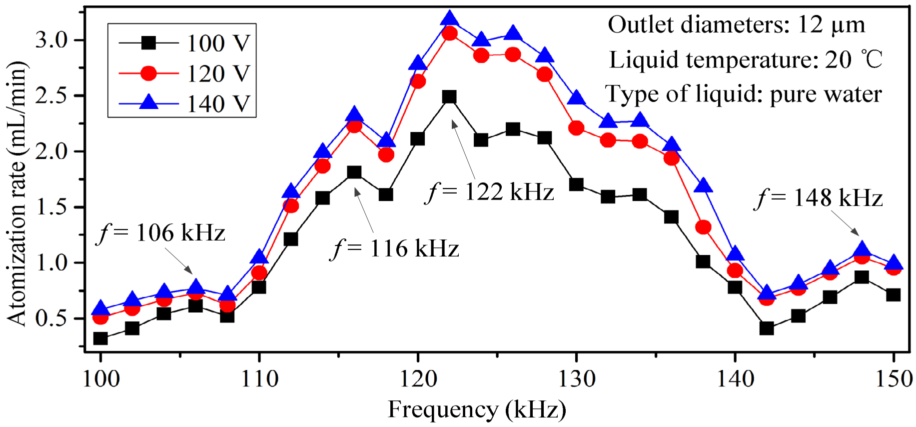

Figure 9. Relationship between atomization rate and frequency.

Table 2. Atomization rates at different resonance frequencies, when the driving voltage is 120 V.

Frequency (kHz)	Atomization Rate (mL/min)
106	0.73
116	2.23
122	3.06
148	1.05

According to the comparisons among the vibration modes of several different resonance points, during the progress of driving frequency at 121.1 kHz, the micro-tapered aperture volume had the highest variation rate. This gives rise to a higher variation rate of the tapered angle and a greater difference between the forward and reverse flow resistance, and further leads to a higher atomization rate. Furthermore, in combination with the data recorded in Figure 5, it can be seen that there were some deviations between the four resonance frequencies obtained in the frequency sweep and the four peak frequencies in the atomization. This is because the atomizer was in a no-load state during the frequency sweep experiment. Additionally, during the atomization experiment, due to the action of the liquid on the piezoelectric vibrator, the resonance frequency experienced some variations, and thus resulted in some deviations in the resonance points and the optimal atomization frequency.

Figure 10 shows the relationship between the atomization rate and voltage at different resonance frequencies. The liquid used in the experiment was pure water at room temperature (25 °C), and the pore diameter of the micro-tapered aperture was 12 μm. It can be observed that obvious atomization started to emerge when the driving voltage reached 60 V. All of the atomization rates at these four resonance frequencies increased with the increase in driving voltage. Table 3 shows the atomization rates at different driving voltages, when the driving frequency was set as 122 kHz. This can be explained by the fact that as the applied voltage increased, the variation of the micro-tapered aperture volume also increased, leading to the increase of the aperture angle variation; as a result, the difference between the forward and reverse flow resistance of the micro-tapered aperture also increased, thus exerting a more obvious pumping effect. According to Equation (4), a micro-tapered aperture produces a higher atomization rate in this case.

Figure 11 shows the outlet diameters of micro-tapered apertures used in this experiment. Figure 12 exhibits the relationship between the atomization rate and the micro-tapered aperture size under the same working condition. The liquid used in the experiment was pure water at room temperature (25 °C), and the working frequency was 122 kHz. Under the same working conditions, the larger the outlet diameter of the micro-tapered aperture, the higher the atomization rate will be. Table 4 shows the atomization rate of different micro-tapered aperture sizes under the same conditions. The micro-tapered apertures basically had a constant inlet diameter. When the outlet diameter increased, the aperture volume also increased. Under the same driving conditions, the variation of the micro-tapered aperture volume becomes higher, leading to a stronger pumping effect and a higher atomization rate.

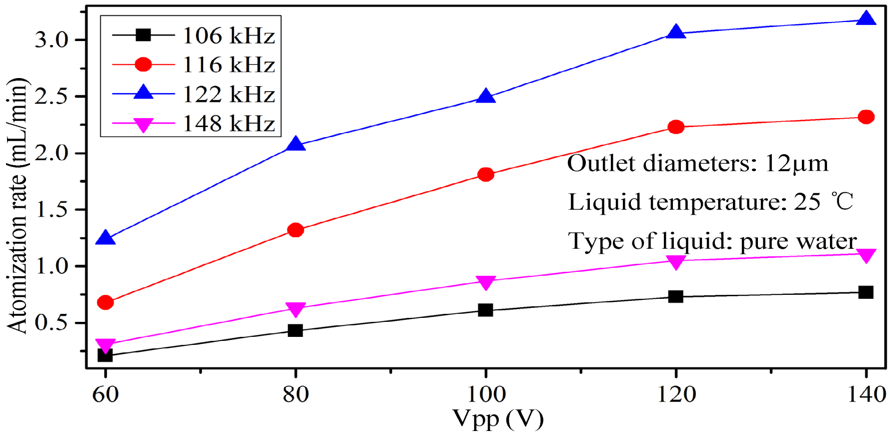

Figure 10. Relationship between the atomization rate and frequency.

Table 3. Atomization rates at different driving voltages, when the driving frequency is 122 kHz.

Voltage (V)	Atomization Rate (mL/min)
60	1.24
80	2.07
100	2.49
120	3.06
140	3.18

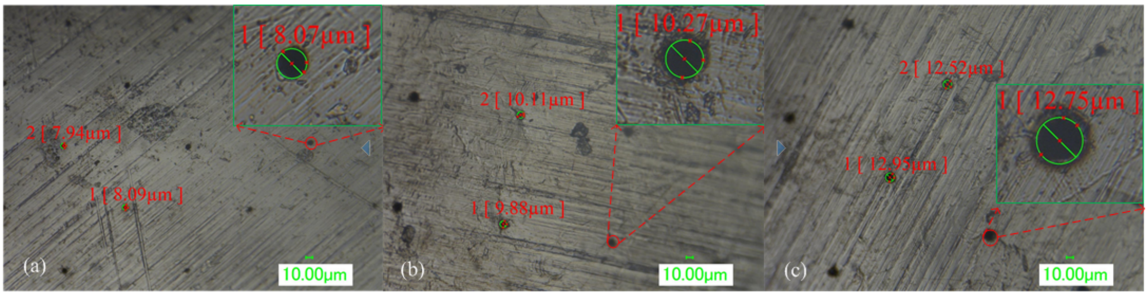

Figure 11. Outlet diameters of the micro-tapered apertures.

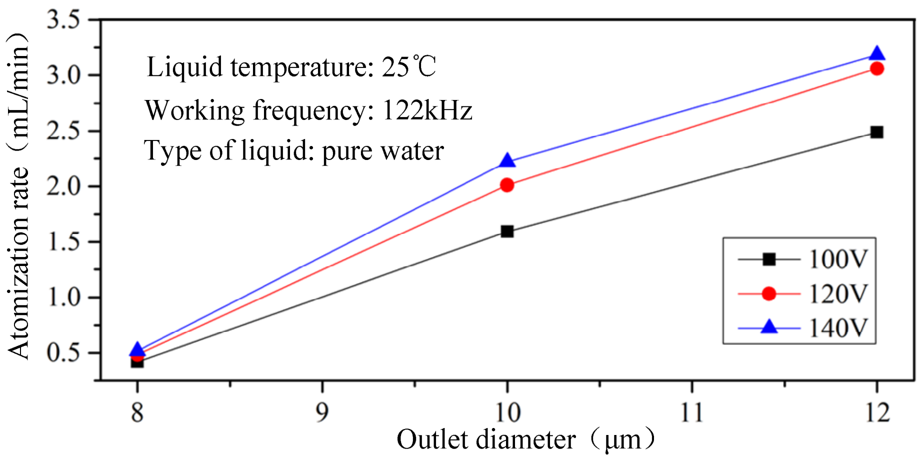

Figure 12. Relationship between the atomization rate and micro-tapered aperture size.

Table 4. Atomization rate of different micro-tapered aperture sizes.

Micro-Tapered Aperture Size (μm)	Atomization Rate (mL/min)
8	0.73
10	2.05
12	3.06

In order to verify the effect of liquid temperature on atomization rate, pure water with temperatures of 10 °C, 15 °C, 20 °C, 25 °C, and 30 °C was applied accordingly. The outlet diameter of the used micro-tapered aperture was 12 μm, and the driving frequency of the atomizer was 122 kHz. Figure 13 shows the relationship between the atomization rate and liquid temperature. Table 5 shows the atomization rate of pure water at different temperatures under the same conditions. It indicated that under the same working conditions, the higher the liquid temperature is set, the higher the atomization rate achieved. This phenomenon can be explained as follows: when the states have the same driving signal, micro-tapered aperture, and liquid concentration, a higher temperature can lead to larger gaps and smaller attraction between the liquid's molecules. Additionally, such larger gaps and smaller attraction could further make the viscosity of the liquid decrease and the Reynolds number of the liquid increase, which weakens the flow resistances of the micro-tapered aperture. Thereby, it is easier for liquid to pass through the micro-tapered aperture and produce a higher atomization rate. Under the same conditions, the higher the liquid temperature reaches, the higher the atomization rate of the aperture achieved.

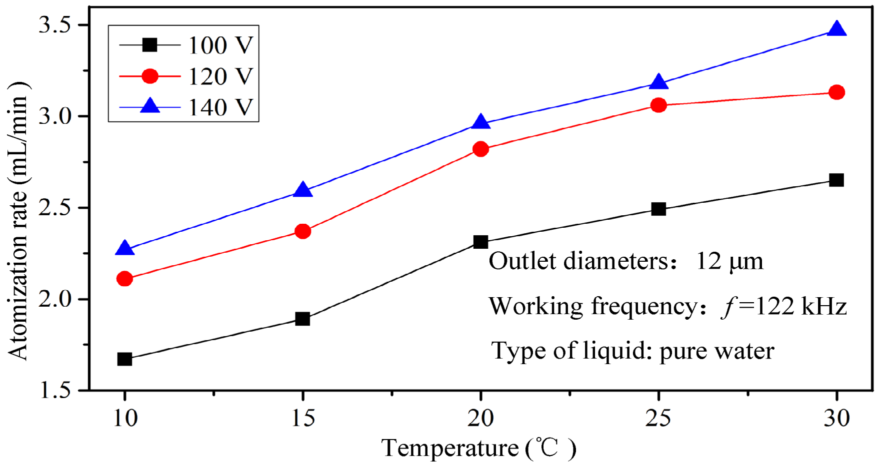

Figure 13. Relationship between the atomization rate and temperature.

Table 5. Atomization rate of pure water at different temperatures.

Temperature (°C)	Atomization Rate (mL/min)
10	2.11
15	2.37
20	2.82
25	3.06
30	3.13

In order to verify the effect of solution concentration on atomization rate, the NaCl solutions with different concentrations of 5%, 10%, 15%, and 20% were prepared, respectively. The outlet diameter of the micro-tapered aperture was 12 μm. The driving frequency of the atomizer was 122 kHz, and the liquid temperature was 25 °C. Figure 14 shows the relationship between the atomization rate and liquid concentration. Table 6 presents the atomization rates at different concentrations of NaCl solution under the same conditions and revealed that under the same working conditions, a lower atomization rate is obtained as a higher liquid concentration is applied. The explanation responsible for this phenomenon is given as follows: under a state with the same parameters including the driving signal, micro-tapered aperture, and the liquid's temperature, the higher liquid concentration means a higher solute content in the solution, producing a higher viscosity of the liquid and a smaller Reynolds number of the liquid. The higher viscosity and smaller Reynolds number can further strengthen the flow resistances of the micro-tapered aperture, which makes it more difficult for liquid to pass through the micro-tapered aperture and thus generate a lower atomization rate. Consequently, under the same experimental conditions, a higher liquid concentration used here could induce a lower atomization rate of the aperture.

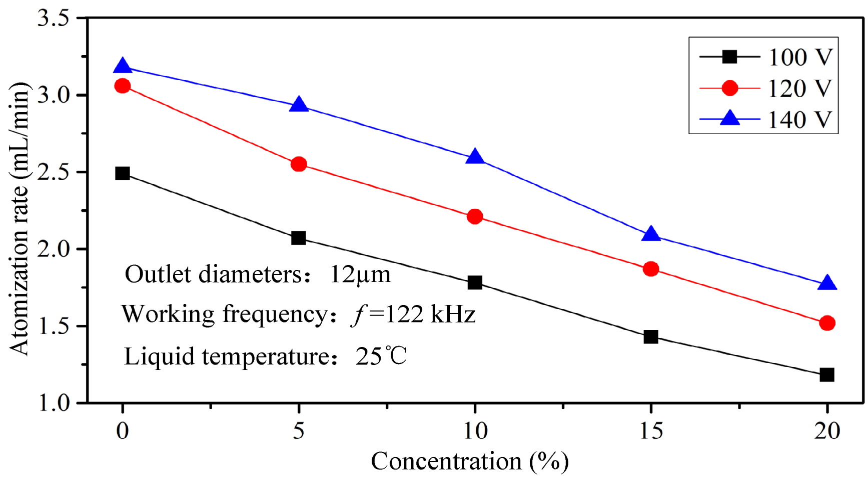

Figure 14. Relationship between the atomization rate and liquid concentration.

Table 6. Atomization rates at different concentrations of NaCl solution.

Concentration (%)	Atomization Rate (mL/min)
0	3.06
5	2.55
10	2.21
15	1.87
20	1.52

6. Conclusions

In this study, the root cause of atomization can be ascribed to two aspects: one is the periodic variation of the micro-tapered aperture volume, and the other is the difference between the forward and reverse flow resistance. For simplification, it is proposed that the micro-tapered aperture can be regarded as a micron-sized tapered flow tube valveless piezoelectric pump. The vibration mode characteristics of the piezoelectric vibrator were simulated using ANSYS software, and the optimal resonant frequency was confirmed as the value of 121.1 kHz. Through measuring the atomization rates at different working frequencies (f), it was found that the f set as a value of 122 kHz corresponds to achieving the maximum atomization rate. By investigating the relationship between atomization rate and voltage at the resonance frequency, it revealed that the atomization rate increased with the increase of the driving voltage. In addition, the micro-tapered apertures of three different outlet diameters were used to measure their atomization rates, and it can be observed that the atomization rate increased with the increase in the micro-tapered aperture diameter. When the atomization rates were measured at different temperatures, the atomization rate increased with the increase in temperature; by changing the liquid concentration, it can be seen that the atomization rate increased with an increase in the liquid concentration. As a conclusion, the root cause of the variation experienced by the atomization rate contributed to the variation experienced by the flow resistance.

Author Contributions: Q.Y. proposed the study; Q.Y. carried out experiments; Q.Y., W.S., and J.Z. analyzed the data; Q.Y. wrote the manuscript; W.S. and J.Z. modified the manuscript. All authors have read and agreed to the published version of the manuscript.

Funding: This research was funded by National Natural Science Foundation of China (51375227).

Conflicts of Interest: The authors declare no conflict of interest.

References

1. De Heij, B.; van der Schoot, B.; Bo, H. Characterisation of a fL droplet generator for inhalation drug therapy. *Sens. Actuators A Phys.* **2000**, *85*, 430–434. [CrossRef]
2. Li, G.; Hu, J.; Hao, X. Application and Research of Swirling Curtain Dust Collection Technology in Mines. *Appl. Sci.* **2020**, *10*, 2005. [CrossRef]
3. Zhang, S.; Campagne, C.; Salaün, F. Preparation of n-Alkane/Polycaprolactone Phase-Change Microcapsules via Single Nozzle Electro-Spraying: Characterization on Their Formation, Structures and Properties. *Appl. Sci.* **2020**, *10*, 561. [CrossRef]
4. Forrest, S.R. The path to ubiquitous and low-cost organic electronic appliances on plastic. *Nature* **2004**, *428*, 911–918. [CrossRef] [PubMed]
5. Awais, M.N.; Muhammad, N.M.; Navaneethan, D. Fabrication of ZrO2 layer through electrohydrodynamic atomization for the printed resistive switch (memristor). *Microelectron. Eng.* **2013**, *103*, 167–172. [CrossRef]
6. Ion, T.; Natacha, R.; Naif, A. Osseointegration of porous apatite-wollastonite and poly (lactic acid) composite structures created using 3D printing techniques. *Mater. Sci. Eng. C* **2018**, *90*, 1–7.
7. Carnesanchez, A.; Imaz, I.; Canosarabia, M. A spray-drying strategy for synthesis of nanoscale metal-organic frameworks and their assembly into hollow superstructures. *Nat. Chem.* **2013**, *5*, 203–211. [CrossRef]
8. Lu, C.F.; Fu, C.C.; Yang, J.C. Traveling wave driven micro-dispenser for CPU cooling application. In Proceedings of the 2006 IEEE Ultrasonics Symposium, Vancouver, BC, Canada, 3–6 October 2006; pp. 54–57.
9. Basaran, O.A.; Haijing, G.; Pradeep, P. Nonstandard inkjets. *Annu. Rev. Fluid Mech.* **2013**, *45*, 85–113. [CrossRef]
10. Wang, H.C.; Yang, L.J.; Liu, J. Controlled Encapsulation of Micron-Sized Beads in a Droplet Based on Pulse Inertia Force Driving of Micro-Fluids. *Key Eng. Mater.* **2015**, *645–646*, 1009–1015. [CrossRef]
11. Zhou, J.; Pang, H.F.; Garcia-Gancedo, L. Discrete microfluidics based on aluminum nitride surface acoustic wave devices. *Microfluid Nanofluid.* **2015**, *18*, 537–548. [CrossRef]
12. Pan, C.T.; Shiea, J.; Shen, S.C. Fabrication of an integrated piezo-electric micro-nebulizer for biochemical sample analysis. *J. Micromech. Microeng.* **2007**, *17*, 659–669. [CrossRef]
13. Zhang, J.; Yan, Q.; Sun, W. Advances in piezoelectric atomizers. *Trans. Nanjing Univ. Aeronaut. Astronaut.* **2020**, *37*, 76–90.
14. Maehara, N.; Ueha, S.; Mori, E. Influence of the vibrating system of a multipinhole-plate ultrasonic nebulizer on its performance. *Rev. Sci. Instrum.* **1986**, *57*, 2870–2876. [CrossRef]
15. Toda, K.; Ishii, J. Operation Performance of Self-Oscillation Ultrasonic Vibrating Device for Liquid Atomization. *Jpn. J. Appl. Phys.* **1995**, *34*, 5332–5334. [CrossRef]
16. Perçin, G.; Levin, L.; Khuri-Yakub, B.T. Piezoelectrically actuated droplet ejector. *Rev. Sci. Instrum.* **1997**, *68*, 4561–4563. [CrossRef]
17. Perçin, G.; Khuri-Yakub, B.T. Piezoelectric droplet ejector for ink-jet printing of fluids and solid particles. *Rev. Sci. Instrum.* **2003**, *74*, 1120–1127. [CrossRef]
18. Roche, P.E.; Hansson, A.; Khuri-Yakub, B.T. Control of a drop-ejector used as photo-resist dispenser. In Proceedings of the VARADAN V V 5th Annual International Symposium on Smart Structures and Materials, San Diego, CA, USA, 1–5 March 1998; Volume 3323, pp. 446–454.
19. Lam, K.H.; Chan, H.L.W.; Luo, H.S. Piezoelectrically actuated ejector using PMN-PT single crystal. *Sens. Actuators A Phys.* **2005**, *121*, 197–202. [CrossRef]
20. Shen, S.C.; WANG, Y.J.; CHEN, Y.Y. Design and fabrication of medical micro-nebulizer. *Sens. Actuators A Phys.* **2008**, *144*, 135–143. [CrossRef]
21. Shen, S.C. A new cymbal-shaped high power microactuator for nebulizer application. *Microelectron. Eng.* **2010**, *87*, 89–97. [CrossRef]

22. Hua, C.; Cheng, W.; Peng, Y. Experimental study on optimal spray parameters of piezoelectric atomizer based spray cooling. *Int. J. Heat Mass Transf.* **2016**, *103*, 57–65.
23. Tsao, C.W.; Lei, I.C.; Chen, P.Y. A piezo-ring-on-chip microfluidic device for simple and low-cost mass spectrometry interfacing. *Analyst* **2018**, *143*, 981–988. [CrossRef] [PubMed]
24. Cai, Y.; Zhang, J.; Zhu, C. Theoretical Calculations and Experimental Verification for the Pumping Effect Caused by the Dynamic Micro-tapered Angle. *Chin. J. Mech. Eng.* **2016**, *29*, 615–623. [CrossRef]
25. Cai, Y.; Zhu, C. Study on the Cooling Performance of Piezoelectric Micro-aperture Atomizer. *Refrig. Air Cond.* **2019**, *33*, 221–227.
26. Cheng, Y.P.; Wang, F.; Xu, J.L. Numerical investigation of droplet spreading and heat transfer on hot substrates. *Int. J. Heat Mass Transf.* **2018**, *121*, 402–411. [CrossRef]
27. Legeune, M.; Chartier, T.; Noguera, R. Ink-jet printing of ceramic micro-pillar arrays. *J. Eur. Ceram. Soc.* **2009**, *29*, 905–911. [CrossRef]
28. Vecellio, L. The mesh nebuliser: A recent technical innovation for aerosol delivery. *Breathe* **2006**, *2*, 252–260. [CrossRef]
29. Yan, Q.; Zhang, J.; Huang, J. Effect of vibration characteristics on the atomization rate in a micro-tapered aperture atomizer. *Sensors* **2018**, *18*, 934. [CrossRef]
30. Zhang., J.; Yan, Q.; Huang, J. Experimental Verification of the Pumping Effect Caused by the Micro-Tapered Hole in a Piezoelectric Atomizer. *Sensors* **2018**, *18*, 2311. [CrossRef]
31. Yan, Q.; Wu, C.; Zhang, J. Effect of the dynamic cone angle on the atomization performance of a piezoceramic vibrating mesh atomizer. *Appl. Sci.* **2019**, *9*, 1386. [CrossRef]
32. Olsson, A.; Stemme, G.; Stemme, E. Numerical and experimental studies of flat-walled diffuser elements for valve-less micropumps. *Sens. Actuators A Phys.* **2000**, *84*, 165–175. [CrossRef]
33. White, F.M. *Fluid Mechanics*; McGraw-Hill: New York, NY, USA, 2003; p. 866.
34. Zhang, J.; WangYing, F.J. Advances in technologies of piezoelectric pumping with valves. *Trans. Nanjing Univ. Aeronaut. Astronaut.* **2016**, *33*, 260–273.